Plasma electrostatic wave dispersion solution for arbitrary ion distributions

I.H. Hutchinson

June 20, 2024

Abstract

A method is described to solve numerically the dispersion relation and hence investigate stability of arbitrary ion distributions to longitudinal electrostatic oscillations in the ion-acoustic range of velocities. Several subtleties arise that are bypassed in the historic analytic treatments. A dimensionless formulation is implemented that gives robust graphical interpretation and allows direct solution and intuitive display. It is applied to a range of different electrostatic waves and instabilities.

1 Background Theory

The longitudinal relative susceptibility to linear waves ($\propto \exp i(\boldsymbol{k}.\boldsymbol{x} - \omega t)$) that are presumed to have real wave-vector $\boldsymbol{k}$ and possibly complex frequency ω, for a uniform unmagnetized plasma or when the $\boldsymbol{k}$-direction is parallel to the magnetic field is

$$\chi = \sum \chi_j \quad \text{with} \quad \chi_j = -\frac{\omega_{pj}^2}{k^2} \int \frac{\partial f_j}{\partial v} \frac{1}{v - v_p} dv \tag{1}$$

where j denotes the species, $q_j = Z_j e$ is its charge, n_j its density, $\omega_{pj}^2 = n_j q_j^2/\epsilon_0 m_j$ its plasma frequency squared, v the velocity in the parallel ($\mathbf{k}$) direction, f_j the *normalized* one-dimensional parallel velocity distribution function (such that $\int f_j dv = 1$), and v_p is the phase velocity

$$v_p \equiv \omega/k. \tag{2}$$

The integral must be performed using the standard Landau prescription along a contour below the pole at v_p in the complex v-plane.

It is convenient to introduce an energy scale expressed as an effective temperature T_0. In terms of this temperature, the Debye length is $\lambda_D = \sqrt{\epsilon_0 T_0/e^2 n_e}$ and the sound speed is $c_s = \sqrt{T_0/m_i}$. At this stage one can think of these as corresponding to electron temperature $T_e = T_0$ and ion mass m_i. However, we will later sometimes consider T_e to be variable, independent of T_0. In terms of these energy scaled parameters we can write

$$k^2 \lambda_D^2 \chi_j = -Z_j^2 \frac{m_i}{m_j} c_s^2 \int \frac{\partial f_j}{\partial v} \frac{1}{v - v_p} dv \ . \tag{3}$$

We note that the right hand side of this expression, for given plasma parameters, is a function only of the complex phase velocity v_p, not of k and ω independently. Expressed in this way, we can see that the dispersion relation is determined by the sum of distribution functions (differentiated and) multiplied by Z_j^2/m_j integrated over a single velocity space. One can illustrate this by plotting the sum of the distributions so weighted. An example is

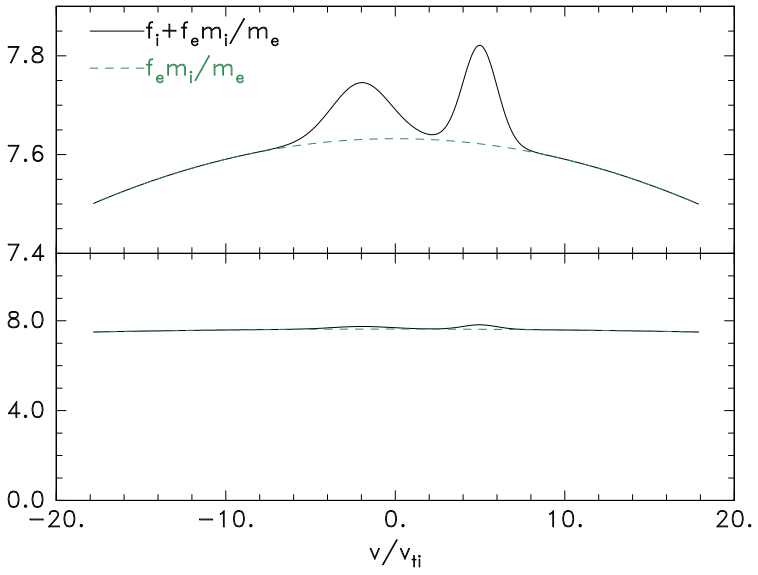

Figure 1: Combined velocity distribution weighted by $1/m_j$, which could be used to determine stability by the Penrose criterion.

Fig. 1. It has been plotted twice; the lower panel avoids the suppressed zero of the upper panel, so as to emphasize the fact that the ion susceptibility arises as a small perturbation on top of a nearly flat electron contribution. The stability of the combined distribution $f_c(v) = f_i(v) + f_e(v)m_i/m_e$ could be analysed by the Penrose criterion, namely that there are unstable modes if and only if there exists a real v_m such that $f_c(v_m)$ is a (local) minimum and $\int [f_c(v) - f_c(v_m)]/(v - v_m)^2 dv > 0$. The integral condition amounts to requiring the local minimum to be deep enough compared with the surrounding distribution. In the context of ion-ion instabilities, one can see that the higher the central f_e is, the less relatively deep a given ion distribution minimum is. Thus lower electron temperature (which makes f_e higher) tends to stabilize the combined distribution. This effect is *not* a result of electron Landau damping. We develop here a way to to understand the problem more quantitatively, yet still giving an intuitive graphical rendering in velocity space.

The dispersion relation for (electrostatic) longitudinal waves is

$$\epsilon = 1 + \chi = 0 \ , \quad \text{or} \quad \chi = -1 \ . \tag{4}$$

Solving it can be approached by finding those phase velocities $v_p = \omega/k$ for which the imaginary part of $k^2\lambda_D^2\chi$ (and hence of χ) vanishes. If the corresponding real part, denoted $\Re(k^2\lambda_D^2\chi)$, for those v_p is negative, then there exists a real k for which $\Re(\chi) = -1$ and the

dispersion relation is solved. However, for v_p such that $\Re(k^2\lambda_D^2\chi) > 0$, no solution exists. If we are therefore able to evaluate the integrals to obtain $k^2\lambda_D^2\chi_j$ at relevant values of v_p, the above approach provides an algorithm for solving the dispersion relation.

In analytic treatments of this problem, convenient analytic representations of the ion distribution functions are generally used. They provide closed-form expressions for the integrals, often in terms of the (Fried and Comte) plasma dispersion function which arises for Gaussian distributions. The present work addresses the more general problem when the ion distribution functions are prescribed in arbitrary numerical terms.

2 Integrating the Susceptibility

2.1 Electron Susceptibility

In principle the electron distribution might be arbitrary as well as the ion distribution. However, the generally very different velocity scale of the electron distribution means that for the exploration of waves in the ion-acoustic frequency range, the electrons' response is usually defined by the Debye length and the low velocity part of their distribution. Performing detailed numerical integrals over the electron distribution is then neither accurate nor appropriate. Therefore we regard the electrons here as having a Maxwellian distribution. As is well known, the electron susceptibility integrals can then be written

$$k^2\lambda_{De}^2\chi_e = \frac{1}{\sqrt{\pi}}\int \frac{z\mathrm{e}^{-z^2}\,dz}{z-x} = 1 - 2xe^{-x^2}\int_0^x e^{z^2}dz + i\sqrt{\pi}xe^{-x^2} \tag{5}$$

where $x = \omega/k\sqrt{2T_e/m_e}$; the first integral is along the Landau contour. It should be emphasized that the Debye length here λ_{De}, is evaluated using the actual electron temperature T_e, not the scaling temperature T_0 (if it is different). This expression is an embodiment of the plasma dispersion function. In terms of standard functions it can be considered the derivative of $(-i\sqrt{\pi}/2)\exp(-x^2)\mathrm{erfc}(-ix)$. In the ion-acoustic regime with $\bar{v}_i \simeq \bar{v}_e$, χ_e is usually well approximated by an expansion that takes v_p to be small compared with $\sqrt{2T_e/m_e}$, which yields

$$k^2\lambda_D^2\frac{T_e}{T_0}\chi_e = k^2\lambda_{De}^2\chi_e \approx 1 + i\sqrt{\frac{\pi m_e}{2T_e}}\,v_p\ . \tag{6}$$

For frequencies well below the electron gyro-frequency and correspondingly small $k\rho_e \ll 1$ (where ρ_e is the thermal gyro-radius) the one-dimensional expressions can be readily extended to give the required longitudinal electron susceptibility for oblique propagation with respect to the magnetic field when the wave-vector has a component $k_\parallel$ along the magnetic field. Purely parallel electron motion replaces f with parallel distribution $f_\parallel$, and replaces speed v with $v_\parallel$ (and v_p with $v_{p\parallel}$) in equation (3) or (6), and $x = \omega/k_\parallel\sqrt{2T_e/m_e}$ in (5). The k^2 factor multiplying χ_e, which arises from the Laplacian in Poisson's equation, remains the total k. Algebraically, the electron current along B is $j_\parallel = -(q^2i\omega/mk_\parallel^2)\int \frac{df_\parallel}{dv_\parallel}\frac{dv_\parallel}{(\omega/k_\parallel - v_\parallel)}E_\parallel$ and the longitudinal components are $j_k = (k_\parallel/k)j_\parallel$, $E_k = (k/k_\parallel)E_\parallel$. Thus $k^2\lambda_{De}^2\chi_{kk} =$

$-\int \frac{df_{e\parallel}}{dv_\parallel}/(\omega/k_\parallel - v_\parallel)dv_\parallel$ is the longitudinal electron susceptibility contribution. This approximation is appropriate for Lower Hybrid waves and instability. However, McMillan (2006) says that a term $(k_\perp/k)^2(\omega_{pe}/\Omega_e)^2$ should be added to the electron susceptibility to account for incomplete electron magnetization.

Expansion eq. (6) becomes inappropriate for angles that enhance $v_{p\parallel}$ so much as to violate $|x| \ll 1$. Then a full numerical implementation of the Faddeeva function, $\exp(-x^2)\mathrm{erfc}(-ix)$, in eq. (5) must be used. It is also required for large shifts between the electron and ion distributions.

2.2 Ion Susceptibility

The ion integrals of eq (3) must be evaluated numerically along the correct contour and performed so as to avoid large errors from the vicinity of the pole $v = v_p$. If a magnetic field is present, influencing the electron susceptibility, but the frequency is simultaneously much greater than the ion gyro-frequency, then the appropriate ion susceptibility remains unchanged. The distribution to be used is that in the k-direction.

For positive $\Im(v_p)$, the ion integral can be evaluated along the real v-axis, but the numerical errors that arise when $|v - v_p|$ is small are managed more effectively if an analytic integration by parts is first performed to give

$$-\int \frac{\partial f_j}{\partial v}\frac{1}{v - v_p}dv = \int \frac{\partial^2 f}{\partial v^2}\left\{\frac{1}{2}\ln\left[\left(\frac{v - v_{pr}}{v_{pi}}\right)^2 + 1\right] + i\arctan\left(\frac{v - v_{pr}}{v_{pi}}\right)\right\}dv, \quad (7)$$

where v_{pr} and v_{pi} are the real and imaginary parts of v_p. This transformation requires the derivatives to vanish at the end of the integration path, which must be observed in the numerical implementation, by using a sufficiently wide velocity range. The error introduced at low $|v_{pi}|$ by the steep behavior of $(v - v_{pr})/v_{pi}$ is first order in the velocity step size or smaller.

For exactly real v_p, the principal value of the integral can be evaluated after two integrations by parts as

$$\mathcal{P}\int \frac{\partial f_j}{\partial v}\frac{1}{v - v_p}dv = \int \frac{\partial^3 f}{\partial v^3}(v - v_p)(\ln|v - v_p| - 1)dv \quad (8)$$

giving rise to no singular contribution at $v = v_p$. The third derivative of f can use simple finite differences. Half of the residue,

$$2\pi i \left.\frac{\partial f}{\partial v}\right|_{v=v_p}, \quad (9)$$

at the pole must be added.

For negative imaginary part of v_p we require numerical analytic continuation of $f(v)$. If the integral path is, as before, along the real-v axis, then the full residue at the pole, eq (9), must be added to it, requiring $\frac{\partial f}{\partial v}\big|_{v_p}$ to be known at complex values of v_p. Perhaps the most straightforward way to perform the continuation is by Fourier transforming f. If $f(v)$ is known along the real axis, then its Fourier transform can be evaluated:

$$F(p) = \int_{-\infty}^{\infty} \mathrm{e}^{-ipv} f(v) dv. \tag{10}$$

Then the continuation of $f(z)$ to complex argument z is

$$f(z) = \int_{-\infty}^{\infty} \mathrm{e}^{ipz} F(p) \frac{dp}{2\pi} \tag{11}$$

Analytic continuation is generally ill-conditioned. Successful numerical implementation requires the spatial frequency bandwidth to be constrained, otherwise short-wavelength errors grow exponentially into the continuation region. One can implement bandwidth limitation using a multiplicative function $B(p)$ that is 1 for small $|p|$ and becomes small for large $|p|$. Then the required derivative can be written

$$\left.\frac{\partial f}{\partial v}\right|_{v=v_p} = \int_{-\infty}^{\infty} ip\ \mathrm{e}^{ipv_p} B(p) F(p) \frac{dp}{2\pi}. \tag{12}$$

This representation is obviously accurate only to the extent that the high-frequencies filtered out by $B(p)$, to suppress noise, are negligible.

It proves advantageous to use a bandwidth filter that depends upon the imaginary part of v_p, designed to limit the magnitude of the real part of the argument of the exponential: ipv_{pi}. This is done by putting in the inverse transform, eq (12):

$$\mathrm{e}^{-pv_{pi}} B(p) = \exp\left(\frac{-pv_{pi}}{1 + (spv_{pi})^2}\right), \tag{13}$$

where s is a constant factor that for noiseless $f(v)$ is generally chosen to be $s \simeq 1/10$. This choice makes the maximum exponent value $1/2s = 5$. Increase of s might be required for noisy $f(v)$.

We suppose that the values of $f(v)$ (real v) are known on a uniform v-grid: $v_n = n\delta v$ with a total of N points. Then discrete fast fourier transforms (from the `fftpack` library) are used. The resulting frequencies are $p_n = n\delta p = n2\pi/(N\delta v)$ and the appropriate finite-duration form of the derivative replaces ip_n in eq (12) with a premultiplying factor $i\sin(n\delta p \delta v)/\delta v$. Thus the back-transform in full is the discrete equivalent of

$$\left.\frac{\partial f}{\partial v}\right|_{(v_{pr}+iv_{pi})} = \int \frac{i\sin(p\delta v)}{\delta v} \mathrm{e}^{ipv_{pr}} \exp\left(\frac{-pv_{pi}}{1 + (spv_{pi})^2}\right) F(p) \frac{dp}{2\pi}. \tag{14}$$

3 Display and Solution

A simple graphical display allows one to read off immediately the solution of the dispersion relation, using a contour plot in complex v_p space of the value of $k^2\lambda^2\chi$, which is determined by the shape of the distribution function.

3.1 Ion Acoustic Waves Displayed as Total χ Contours

One simple way to display the solution for a single electron temperature $T_e = T_0$ is shown in Fig. 2. The velocity units are normalized to the cold ion sound speed $c_s = T_e/m_i$. The upper

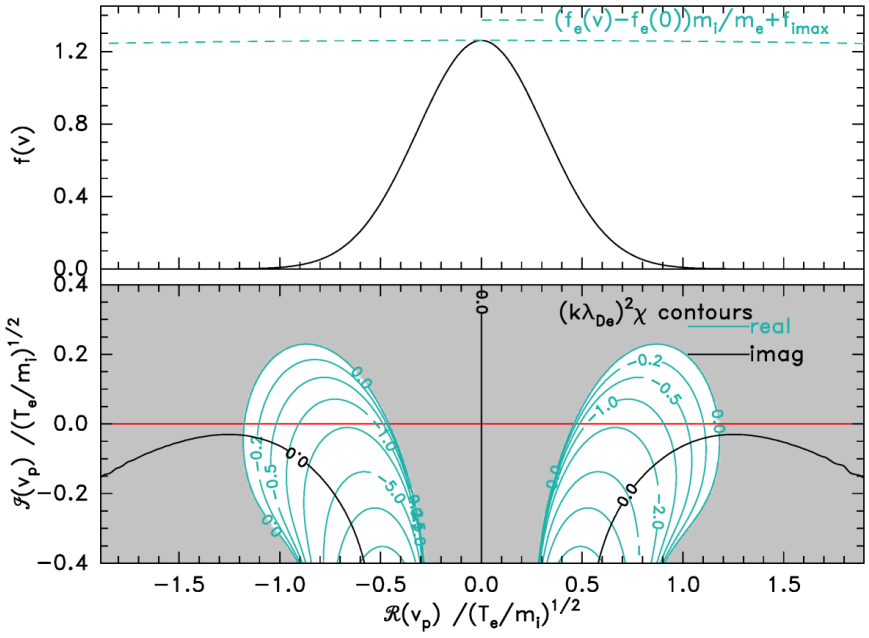

Figure 2: Contours of full susceptibility for $T_e = 10$, $T_i = 1$. At the intersection of the black contour with the green contours, the wave vector k is such that $k\lambda_{De}$ equals the square root of minus the green contour's value.

panel shows the ion distribution, a simple Maxwellian. A green dashed line is added, which shows the deviation of the electron distribution from its peak value $(f_e(v) - f_e(0))m_i/m_e$ scaled by the mass ratio. It shows that the electron distribution ($T_e = 10$ here) hardly varies across the velocity range of the ion distribution. The lower panel plots contours of the full susceptibility in the form $(k\lambda_{De})^2\chi$ where $\chi = \chi_i + \chi_e$. The black contour is where the imaginary part is zero. The green contours are labelled with values of the real part. They are given only for negative values. In the gray shaded region the real part is positive and no solution of the dispersion relation exists. Since the dispersion relation is $\chi = -1$, the solution for a particular value of $k\lambda_{De}$ occurs at the intersection of the black contour with the green contour corresponding to a value $\Re(k^2\lambda_{De}^2\chi) = -(k\lambda_{De})^2$. All such intersections in this case are below the real axis of v_p, showing that ω/k has negative imaginary part and

the waves are damped (k is real and ω has a negative imaginary part) in this case. We shall later encounter unstable cases where the black contour rises above the real v_p axis in the unshaded region.

This display thus provides graphically the entire dispersion relation for all real k, in particular the zero green contour is the long-wavelength ($k \to 0$) limit. The contouring routine

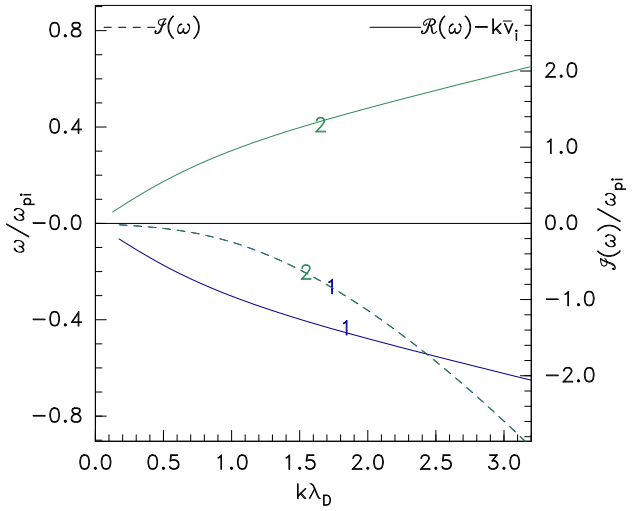

Figure 3: Dispersion plot of ω versus k for simple Maxwellian, $T_e = 10T_i$.

follows the black ($\Im(\chi) = 0$) contour, and as it does so, traces out values from small k, ($\Re(k^2\lambda_{De}^2\chi) \to 0$) to large k, ($\Re(k^2\lambda_{De}^2\chi) \to -\infty$). By collecting those values, and recognizing that $\omega = v_p k = v_p\sqrt{-\Re(k^2\lambda_{De}^2\chi)}/\lambda_{De}$, one can readily construct the corresponding dispersion relation and plot $\Re(\omega)$ and $\Im(\omega)$ as a function of k. Fig. 3 shows the result corresponding to Fig. 2. There are two branches corresponding to negative and positive phase velocity and $\Re(\omega)$ (k is taken positive). By symmetry they both have exactly the same damping factor $-\Im(\omega)$ which makes the two dashed lines plot exactly over one another.

3.2 Alternative Two-Tone Plot Approximation

An alternative way to display an approximation for a range of electron temperatures not necessarily equal to T_0 is the following. We recognize that when the phase velocity v_p (relative to the center of the electron Maxwellian) is small, the electron susceptibility in the dispersion relation can be approximated as

$$k^2\lambda_D^2(\chi_i + 1) = -k^2\lambda_D^2\chi_e \approx -\frac{T_0}{T_e}\left(1 + i\sqrt{\frac{\pi m_e}{2T_e}}v_p\right). \tag{15}$$

The imaginary term in χ_e (electron Landau damping) is smaller by the square root of the inverse mass ratio, and significant mostly at high phase velocity. Neglecting it has the effect of raising the black contour (on which the imaginary part of χ is zero) toward zero at large

$|v_p|$, but it has little effect where f_i is non-negligible. The real part of the dispersion relation is simply

$$k^2\lambda_D^2 = -\Re(k^2\lambda_D^2\chi_i) - T_0/T_e. \tag{16}$$

If k is regarded as a free choice, the dispersion relation can be satisfied at any complex phase velocity at which the right hand side of (16) is positive: $\Re(k^2\lambda_D^2\chi_i)$ is more negative than T_0/T_e, and simultaneously $0 = \Im(k^2\lambda_D^2\chi) \simeq \Im(k^2\lambda_D^2\chi_i)$. The value of k^2 is given by eq. (16) for a root on a contour of known $\Re(k^2\lambda_D\chi_i)$ and T_0/T_e. Consequently, contours in the complex v_p plane of $\Re(k^2\lambda_D\chi_i)$ (which we've shown depends only on the shape of the ion distribution) correspond to contours of $k^2\lambda_D^2$, if T_0/T_e is fixed. But alternatively we can consider a range of different possible T_0/T_e values, and regard the region of existence of solutions as being bounded by contours at which $\Re(k^2\lambda_D^2\chi_i) < -T_0/T_e$. Taking $T_e \to \infty$ gives the largest extent ($\Re(k^2\lambda_D^2\chi_i) < 0$) for which this can be satisfied, but for any other temperature ratio the contour equal to $-T_0/T_e$ bounds the existence region. For example when $T_0/T_e = 1$, $\Re(k^2\lambda_D^2\chi_i) < -1$.

Fig 4 shows what is obtained for the same simple Maxwellian as before, choosing $T_0 = 10T_i$. The light-gray shaded regions are those where $\Re(k^2\lambda_D^2\chi_i)$ is more positive than -1.

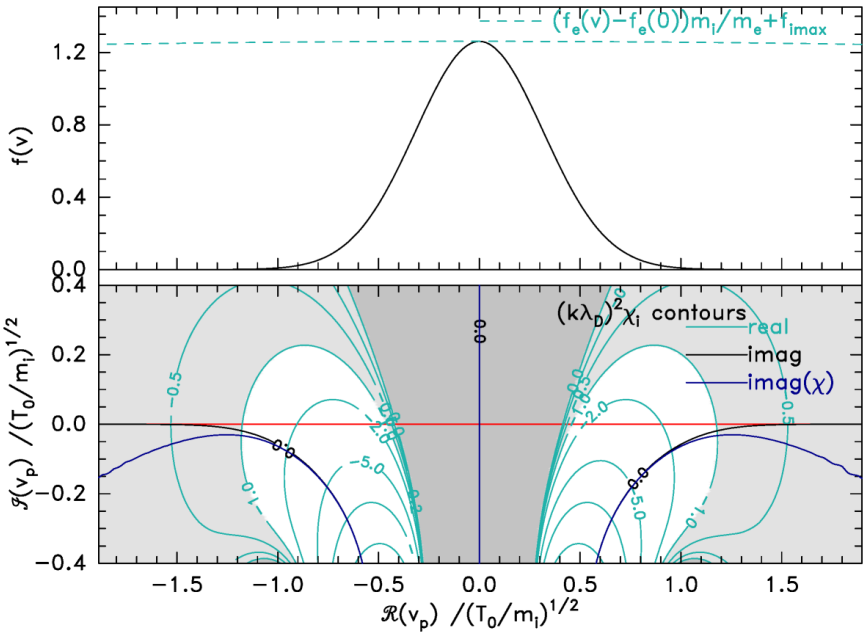

Figure 4: Contour Plot of ion susceptibility from which the dispersion relation can be read. The real-part contour heights are logarithmically spaced, being at minus 0., .2, .5, 1., 2., 5., 10. etc. These values can be interpreted as the T_0/T_e at which each contour is the $k \to 0$ boundary of solution existence. Simple Maxwellian ion distribution with $T_0 = 10T_i$.

Those are regions where no solutions exist for $T_e = T_0$. For that electron temperature, the dispersion relation solutions lie (only) along those segments of the imaginary-part zero-

contour that lie in unshaded regions. Those unshaded regions are actually identical to the unshaded regions of Fig. 2, in so far as the approximation $\Re(k^2\lambda_{De}^2\chi_e) = T_0/T_e$ holds. The real contour values differ from those in Fig. 2 by -1. Although the green and black contours are of χ_i, the actual dispersion relation requires $\Im(\chi) = 0$, using the full $\chi = \chi_i + \chi_e$. By plotting in addition the zero contour of $\Im(\chi)$ (for the case $T_e = T_0$): the blue line, one obtains the full solution (following the blue line and finding its intersections with the green) of the dispersion for that case. The black line is the $\Im(\chi) = 0$ contour ignoring electron Landau damping, which is exact only when $T_e \to \infty$. So the difference between the black and blue contours indicates the degree of approximation involved in ignoring electron Landau damping for $T_0/T_e = 1$. At any electron temperature between T_0 and ∞ the corresponding imaginary contour would lie between the blue and the black curves. At any point along such curves, the real part of $k^2\lambda_D^2\chi_i$ can be read from the green contours that intersect it. Knowing $k^2\lambda_D^2\chi_i$ one can immediately deduce the value of k from eq. (16). The edge of the allowed solution region for a T_e different from T_0 is at the contour where $\Re(k^2\lambda_D^2\chi_i) = -T_0/T_e$. So the green contours can be considered universal for any T_e. For example, if $T_e = 20T_i = 2T_0$, then the -0.5 contour is the allowed solution boundary.

Omission of electron Landau damping hardly affects the black contour in the unshaded region, but it raises it toward $v_{pi} = 0$ further out in the light shaded region. The smallest k solution for $T_e = T_0$: the long wavelength solution, occurs at the boundary with the (light) shaded region where $\Re(k^2\lambda_D^2\chi) = 0$ and $\Re(k^2\lambda_D^2\chi_i) = -1$. In Fig 4, that position is at $\Re(v_p) \approx \pm 1.15 c_s$ because $T_i/T_0 = 0.1$ in this case, and the actual warm-ion acoustic speed for such waves is approximately $\sqrt{(T_e + 3T_i)/m_i}$. If instead $T_e = 2T_0$, the long wavelength root (contour -0.5) has v_p just over 1.5. Or again, if $T_e = 0.5T_0$ the solution boundary is at the -2.0 contour. The imaginary part of v_p is everywhere negative along the solution curve (blue) in this plot, indicating that these waves are damped. The damping rapidly becomes stronger as one moves away from the shaded edge because the real part becomes large (and negative) implying large k, and thus large ω_i (because $\omega_i = kv_{pi}$).

An important caveat for the alternative two-tone treatment is that the approximations employed are appropriate only for small phase velocity relative to electron thermal velocity. When $v_p/c_s \gtrsim \sqrt{m_i/m_e}/5$ it should not be used.

3.3 Current-driven Instabilities

When both electrons and ions are Maxwellian but their central velocities differ, a current is present. Ignoring the fact that it will perturb the magnetic field, we can still examine electrostatic stability. We choose to express velocities relative to the mean electron velocity, but still in units of the ion acoustic speed.

Ion acoustic instability can be driven by current that corresponds to quite moderate ion velocity shift when the temperature ratio T_e/T_i is high enough. Fig. 5(a) illustrates a case with a moderate ion velocity shift $-10\sqrt{T_i/m_i} = -2.24\sqrt{T_e/m_i}$. The ratio $T_e/T_i = 20$ makes ion Landau damping negligible and the black lines (omitting the imaginary χ_e) are

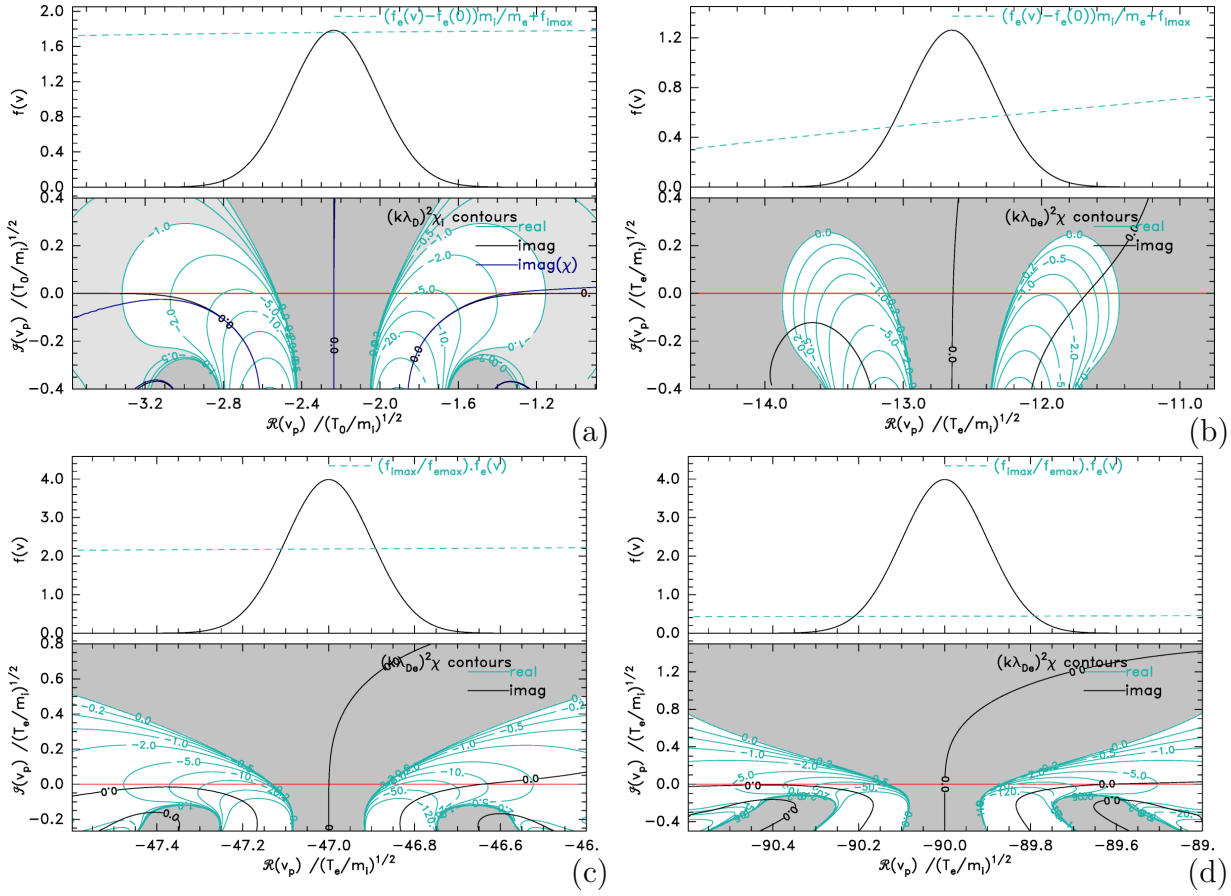

Figure 5: Ion acoustic instability for $T_i = 1$, (a) $T_0 = 20$, $v_i = -10\sqrt{T_i/m_i}$, (b) $T_0 = 10$, $v_i = -40\sqrt{T_i/m_i}$ (c) $T_0 = 100$, $v_i = -470\sqrt{T_i/m_i}$ (d) $T_0 = 100$, $v_i = -900\sqrt{T_i/m_i}$. In (b)-(d) the unapproximated electron susceptibility is used; and f_e scaled to the same height as f_i is plotted, showing the very slight positive df_d/dv) and how far out on the electron Maxwellian the plot is. Cases (c) and (d) are effectively Buneman instabilities accounting for finite ion temperature.

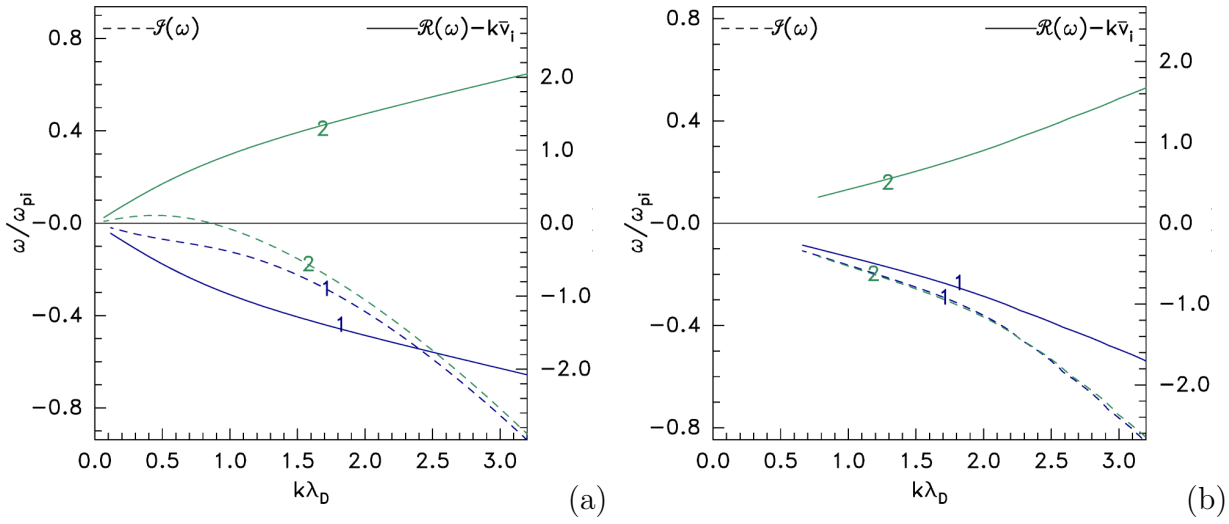

Figure 6: Dispersion curves (a) corresponding to Fig 5(b) and (b) corresponding to Fig 5(d). The real frequencies (solid lines) displayed are in the frame of reference of the mean ion velocity ($\Re(\omega) - k\bar{v}_i$). The curves labelled 2 are the unstable roots with dashed (imaginary) curves rising above zero.

extremely close to the real axis away from the ion distribution region. But including $\Im(\chi_e)$ the positive slope of the electron distribution causes the blue line to rise above the real axis on the right of the ions: unstable growth. This is the current-driven ion acoustic instability. On the left damping occurs. Fig. 5(b) shows a much greater velocity shift, having larger $\Im(v_p)$ even with lower $T_e = T_0 = 10T_i$, but it is a qualitatively similar ion-acoustic wave. Fig. 5(c) and (d), having $T_e = 100T_i$ would be reasonably represented by a fluid ion treatment, and in fact correspond to **Buneman instabilities**. Buneman's original treatment used cold fluid ions.

The main point of this comparison is to show that there is no qualitative distinction between ion-acoustic instability and Buneman instability. From the viewpoint of a Penrose analysis they both arise from the formation of a local minimum in the combined distribution $f_e + (m_e/m_i)f_i$. Or in other words from a positive slope of f_e at phase speeds where the real part of χ is negative, permitting a solution of the dispersion relation (with real k). As the velocity shift magnitude increases, ion acoustic and Buneman instabilities connect continuously.

Fig. 6 shows conventional dispersion curves of ω versus k, expressed in the ion frame, for two of the cases of Fig. 5. The large-shift Buneman regime (b) has faster instability peak growth rate by a factor of approximately 20.

3.4 Positive-slope f_i tail

A different sort of ion distribution is shown in Fig 7, where a relatively long tail of slightly positive slope is added to the Maxwellian bulk (whose temperature is $T_0/30$). The tail induces

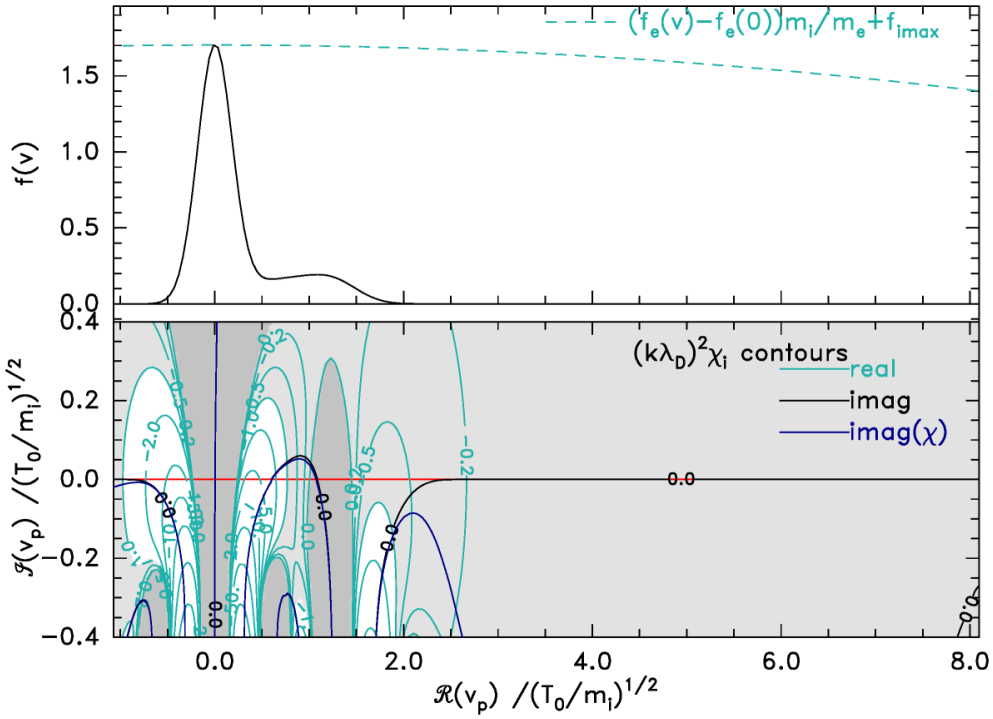

Figure 7: Contour Plot of ion susceptibility for an ion distribution with a long tail of slightly positive slope, showing unstable regions. $T_0 = 30T_i$.

an ion-acoustic instability (sometimes called "ion-ion" but not entirely appropriately in this case), but requires no current (i.e. electron shift) to do so. The instability is in the region where the $\Im(\chi_i) = 0$ contour rises above the real v_p-axis, corresponding to wave growth. The unstable solutions actually exist only near the low-velocity end of the tail for $T_e = T_0$. In the higher-velocity range, although the contour is still at positive v_{pi} it is in the light shaded v_p region where the real part of χ is positive and the dispersion relation cannot be satisfied. This observation is an important corrective to any improper transference of intuition derived from *electron* stability of Langmuir waves. Unstable Langmuir waves exist on an electron-distribution-tail throughout most of the region where its slope is positive. That is not the case for ion-acoustic instability.

Actually a direct quantitative understanding of this difference can be derived from the figure. In the limit $T_e \to \infty$, the electrons contribute negligibly to the total susceptibility. Only the ion contribution need be considered. In that case the dispersion relation (along the black line) is *exactly* the same as it would be for Langmuir waves of electrons of the same distribution (scaling the velocities appropriately, see section 5.1). We see that then the solution region (outside the dark grey shading) extends almost (but actually not quite) to the upper end of the positive slope region. This is exactly the region of Langmuir wave instability for an electron distribution of this shape. So there is a precise analogy between the ion and electron distribution positive-slope Landau growth at $T_e \to \infty$. However, as T_e

is lowered, the electron contribution to χ becomes significant, and causes the solution region to contract towards the lower velocity end of the tail. If T_e becomes less than approximately $T_0/3$, the solution region (whose boundary is then on the ~ -3 contour) no longer contains any positive-$\Im(v_p)$ regions of the $\Im(\chi_i) = 0$ contour. The ion instability disappears. The last phase velocity to remain unstable is where the $\Im(\chi) = 0$ contour crosses the x-axis: $v_p \approx 0.5c_s$. This suppression of ion-ion instability by lowering of T_e is *nothing to do with electron Landau damping*, which is still negligible, as evidenced by the equality of the black and blue curves in this vicinity. It is caused by the real part (not the imaginary part) of the electron susceptibility.

In the opposite direction to the tail, a relatively weakly damped acoustic branch exists. A third branch, which is strongly damped unless T_e is very high, exists just beyond $2c_s$, and some other extremely heavily damped branches of little practical relevance also exist at $\Im(v_p) < -0.3$. Those heavily damped branches are omitted from the $\omega(k)$ dispersion plot of Fig. 8. The branch 2 is now unstable for $k\lambda_D \lesssim 1.4$.

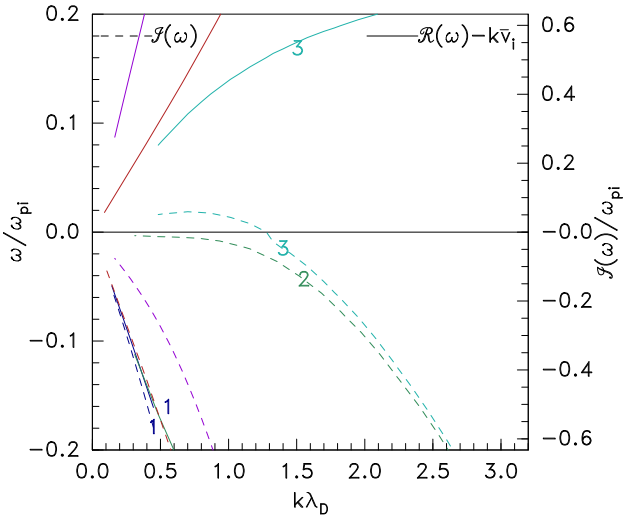

Figure 8: Dispersion curves for the $T_e = T_0 = 30T_i$ case of Fig. 7.

3.5 Two shifted ion populations

Fig. 9 shows an ion distribution with two overlapping humps. The reference temperature is taken as 3 times the temperature of the unshifted hump (the other hump has width corresponding to a temperature 0.6 times lower). When $T_e = T_0$, waves are only just unstable in the distribution minimum near $v_p = 1.2$. Lower T_e would not be unstable. Higher T_e permits greater growth rate, again indicating the importance of T_e in determining stability, but again not arising from electron Landau damping. For five times higher T_e the maximum growth rate of the instability is greatly increased, yet the range of real part of the phase velocities that are unstable is extremely narrow, residing at the bottom of the valley between the humps, where electron Landau damping is unimportant. This near-vertical branch of

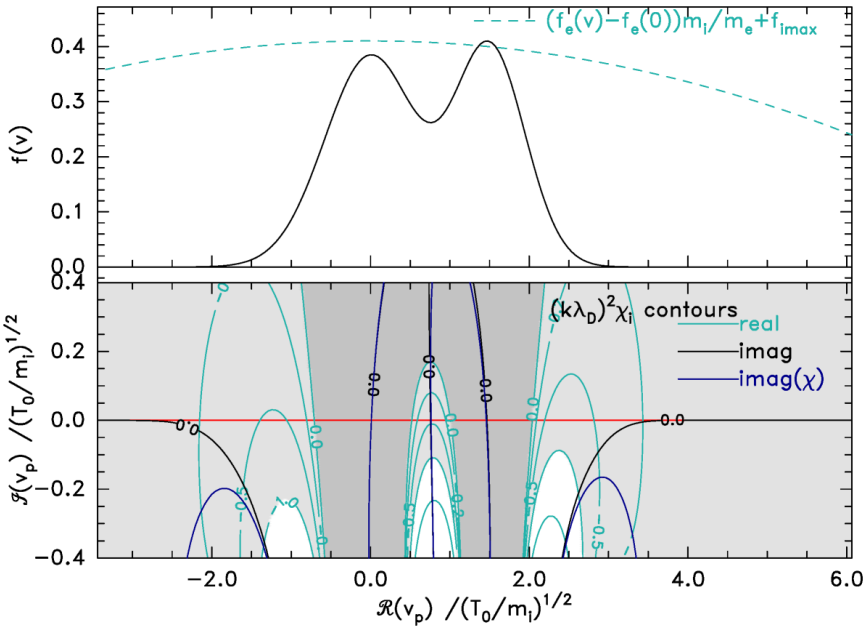

Figure 9: Contour Plot of ion susceptibility for an ion distribution with two humps. T_0 is 3 times the temperature of the unshifted hump. It can be called an ion-ion or ion-two-stream instability.

the imaginary zero-contour is completely separate from the ion-acoustic branches at left and right, which in this case are strongly Landau damped. The instability is therefore clearly not ion-acoustic, and could be called "ion-ion", or perhaps "ion-two-stream".

Fig. 10 shows a case by contrast in which two Gaussian humps have negligible overlap. The stable ion sound branches for the two humps are clearly visible. The centers of the ion humps are separated by just over twice c_s. The result is that the allowed solution regions (unshaded) for $T_e = T_0$ merge in the middle, producing an unstable region along a section of the vertical $\Im(\chi) = 0$ branch. Lower temperatures (e.g. the -2.0 contour, $T_e = 0.5T_0$) don't merge and so do not have unstable solutions, higher temperatures (light gray) have greater extent and growth rate of instability. Generally speaking, humps separated by more than twice the ion sound speed don't lead to instability. Stringer[1] gives a criterion $1.3v_{ti} < \Delta v/2 < \sqrt{T_e/m_i}$ for ion-ion instability when equal Maxwellian ion distributions are separated by velocity Δv.

4 Oblique Propagation

So far the analysis has been of electrostatic waves either in an unmagnetized plasma or propagating parallel to the magnetic field. Moreover here and in subsequent analyses the

[1]T E Stringer, Plasma Physics, **6**, 267-279 (1964).

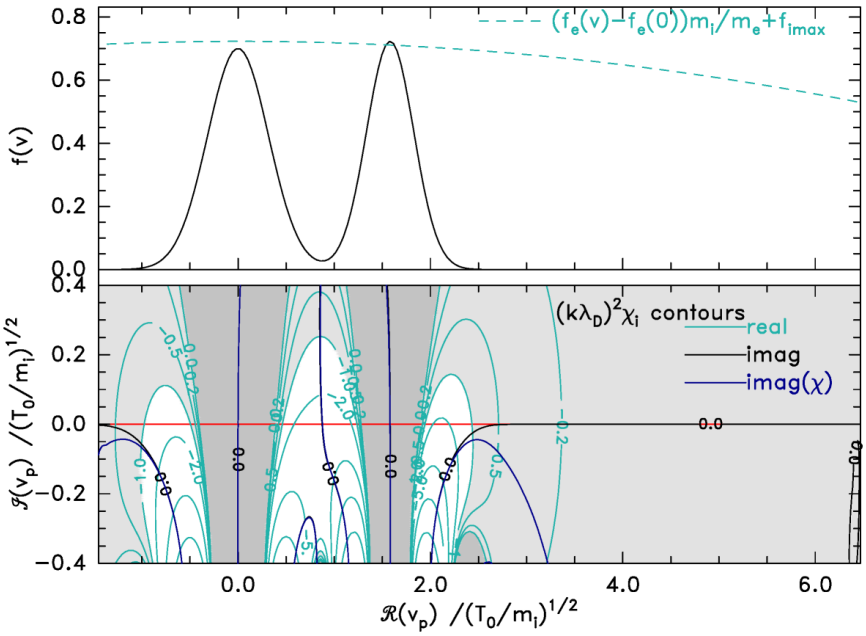

Figure 10: Contour Plot of ion susceptibility for an ion distribution with two well separated Gaussians. T_0 is 10 times the temperatures of the centered ion Gaussian.

distribution function to be used has been the one dimensional distribution, i.e. integrated over velocities perpendicular to the wavevector $\boldsymbol{k}$.

4.1 Beam-like Ion distributions in 3-D

If the ion distribution in three velocity directions were really represented by two shifted but otherwise isotropic finite width beams (e.g. shifted 3-D Gaussians) and the plasma were unmagnetized, then the relevant velocity shift between the beams as viewed in the one-dimensional distribution is equal to the velocity shift in 3-D, $|\boldsymbol{\Delta v}|$, times the cosine of the angle between $\boldsymbol{k}$ and the direction of velocity shift i.e. $\boldsymbol{k}.\boldsymbol{\Delta v}/(k\Delta v)$. If then Δv is large enough in one dimension to avoid ion-ion instability because $\Delta v \gtrsim 2\sqrt{T_e/m_i}$, that does *not* make an unmagnetized plasma stable. Instead we would require $\boldsymbol{k}.\boldsymbol{\Delta v}/k \gtrsim 2\sqrt{T_e/m_i}$ for *all possible propagation directions*. Clearly that can never be satisfied, because we can make the wave vector and shift directions as near to perpendicular as we like.

In general then, unmagnetized plasmas with two widely spaced ion beams are hardly ever completely stabilized against ion-ion instability, because along some angle of propagation relative to the spacing, they are not widely spaced. (However, a spherically symmetric hollow distribution could be stable.)

The most common magnetized situation for oblique propagation of ion waves is that the electron cyclotron frequency is much higher than that of the waves, while the ion cyclotron frequency is much lower. Thus to a first approximation electrons are strongly magnetized,

moving only parallel to the magnetic field, while ions are unmagnetized. Since complete magnetization of electrons changes their susceptibility only by replacing $v,\ v_p$ in the integral by $v_\parallel,\ v_{p\parallel}$, or equivalently making the argument of eq. 5 $x = \omega/k_\parallel\sqrt{2T_e/m_e}$, oblique propagation relative to the magnetic field mostly narrows the effective electron distribution, enhancing electron Landau damping (or growth) at the low speeds typical of ion waves, for constant $f_{ik}(v_k)$. However, as we have just seen, electron Landau damping is a relatively unimportant effect for controlling the ion-ion instability of separated beams. Electrons' more important influence is in setting the height of the combined distribution function and thereby affecting the real part of the susceptibility. That is not changed by magnetizing the electrons at an angle to k.

4.2 Oblique Electron-Ion instability

By contrast, if a positive slope of the electron distribution in the direction away from the mean ion velocity exists at the resonant velocity, as it does for ion-acoustic or Buneman instabilities, giving a local minimum in the combined distribution, the enhancement of parallel *slope* of magnetized electron distribution at oblique propagation can lead to enhanced instability. Oblique propagation for magnetized electrons makes the electron contribution depend on the angle θ between $\mathbf{k}$ and $\mathbf{B}$, because at constant $v_{p\parallel}$, $\partial f/\partial v_k$ is proportional to $1/\cos(\theta) = \sqrt{1 + v_\perp^2/v_\parallel^2}$. Lower Hybrid waves can then experience instability when $\cos(\theta)$ is small. Magnetization of the electrons (but not ions response) makes the Penrose combined distribution $f_i(v_k) + f_{e\parallel}(v_{e\parallel})m_i/m_e = f_i(v_k) + f_{e\parallel}(v_k k/k_\parallel)m_i/m_e$. Then the electron velocity scale of the electron contribution in Figure 1 changes with the propagation angle $\theta = \cos^{-1}(k_\parallel/k)$. The electron contribution becomes narrower in v_k as the corresponding $v_{e\parallel} = v_k/\cos\theta$ increases, but without changing in height. Consequently its derivative with respect to v_k increases.

The direction of the ion distribution components' shift $\boldsymbol{\Delta v}$ is taken as being along $\boldsymbol{B}$, so the same geometrical compression factor $\cos\theta$ applies for ion velocity shifts and electron distribution. However, Lower Hybrid waves in some circumstances must account for an extra partially-magnetized electron response term $\chi_{e\perp} = (\omega_{pe}/\Omega_e)^2\sin^2\theta$ added to the parallel susceptibility $\chi_{e\parallel}$. This term $\chi_{e\perp}$ is not $\propto 1/k^2$, so its relative influence depends on k as well as v_p. However, it is a positive definite real term added to χ_e, so its influence is always to reduce the (unshaded) area of the contour plot in which $\Re(k^2\lambda_{De}\chi) < 0$, no matter the value of k. It does not change $\Im(k^2\lambda_{De}\chi)$ so the contour of $\Im(k^2\lambda_{De}\chi) = 0$ remains unchanged. Therefore addition of $\chi_{e\perp}$ reduces the range of phase-velocities over which solutions of the dispersion relation exists, and cannot itself induce instability in an otherwise stable plasma.

5 Electron Waves

5.1 Electron Langmuir Waves

The same display can also calculate the dispersion of electron Langmuir waves. Consider a high-frequency situation in which χ_i can be ignored and χ_e is the electron susceptibility for an arbitrary electron distribution function. Regard that distribution as being given by the upper frame of the plot (what in the ion acoustic analysis is the ion distribution function). Take the reference velocity to be $\sqrt{T_0/m_e}$. The dispersion relation is then $\chi_e = -1$. Since the shape of the distribution function and the complex v_p together determine the value of $k^2\lambda_D^2\chi_e$ (eq. 3), the dispersion relation is satisfied for some real value of k at points in v_p space where the value of the real part of $k^2\lambda_D^2\chi_e$ is negative and the value of its imaginary part is zero, just as before. Therefore we exchange the roles of electrons and ions. We consider the plot to be for electron susceptibility. The solution of the dispersion relation is where the imaginary part is zero and the real part is negative. (Using the special value switch `-T99`, is programmed turn off extra Maxwellian electron influence and to label the plots for electrons rather than ions, as illustrated in Fig. 11.)

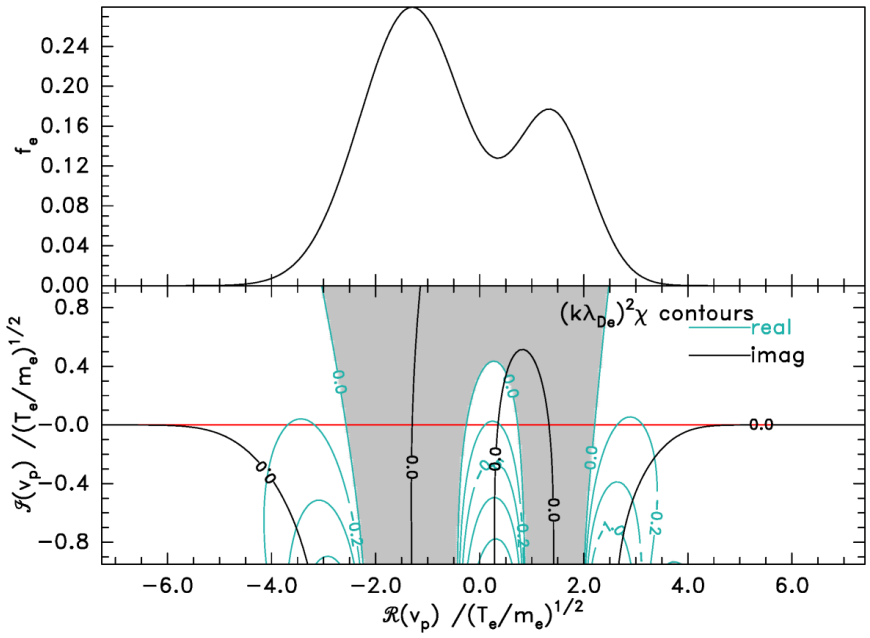

Figure 11: Langmuir wave pure electron case with double humped distribution, giving warm two-stream instability.

This reversal of roles helps one to understand the qualitative difference between ion acoustic stability and Langmuir stability. It lies purely in the fact that non-zero electron susceptibility shifts the real contours of the ion acoustic case. When $T_e/T_0 \to \infty$, and χ_e becomes negligible, the ion acoustic instability is exactly equivalent to the Langmuir stability with appropriately scaled velocity.

5.2 Electron-acoustic waves

A type of wave occurring in non-Maxwellian electron distributions with two components of different temperatures is often called the electron-acoustic wave. There is nothing particularly different about such waves except that normal Langmuir waves are strongly damped unless their phase speed substantially exceeds the electron thermal speed. That criterion, $\omega/k \gg \sqrt{T_e/m_e}$, is equivalent to $k\lambda_{De} \ll 1$, taking $\omega \simeq \omega_{pe}$. By adding a hot electron component when prescribing electrons only, an electron-acoustic mode can be permitted that is weakly damped or growing. Figure 12 illustrates a case. It is no coincidence that this figure looks rather similar to the ion-tail case Fig. 7. It is debatable whether there is any meaningful distinction between an "electron acoustic instability" and an extended-"bump-on-tail" instability. Their mechanisms are of course the same.

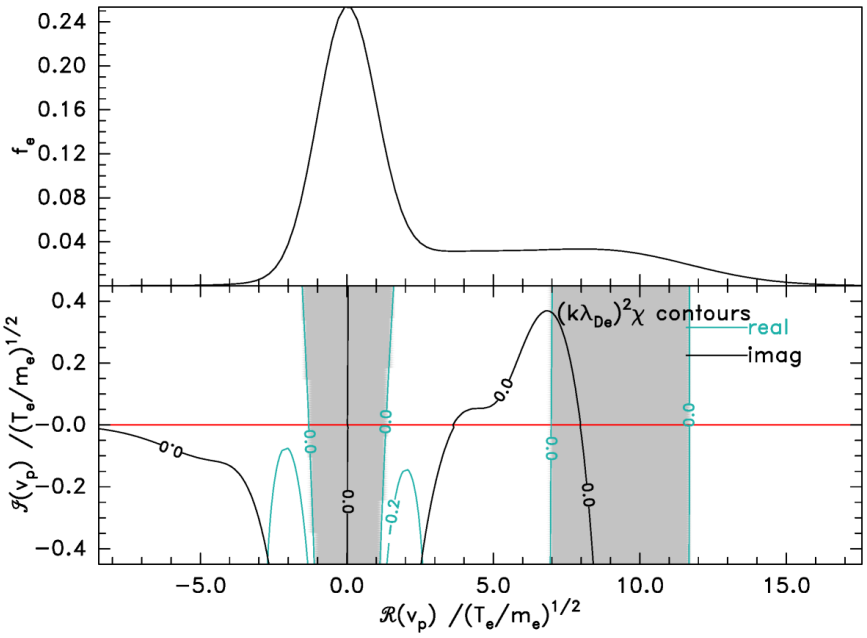

Figure 12: Unstable electron-acoustic mode ignoring ion response.

6 Group Velocity

The plots automatically give the phase velocity of the wave, since they are plots on the real and imaginary axes of v_p. The group velocity corresponding to waves on these solution contours can be found as follows.

$$v_g = \frac{d\omega}{dk} = \frac{d}{dk}(v_p k) = v_p + \frac{k}{dk/dv_p} = v_p + \frac{k\lambda_D}{d(k\lambda_D)/dv_p} \tag{17}$$

We substitute the value $k^2\lambda_D^2$, from eq. (16), which is what is contoured in the plots. And we recognize that the second term by which v_g differs from v_p is simply half the scale

length of the variation of $k^2\lambda_D^2$ as a function of v_p. Since (except for the zero level) the contours are logarithmic in the ratios 1,2,5, the distance between the function's contours is approximately the scale length of the function.

Therefore the value of the group velocity is approximately half way between the contour of $-\Re(k^2\lambda_D^2\chi_i)$ on which it lies and the adjacent contour further from the shaded boundary. In most cases the shift from v_p is small enough to be inconsequential. There will be zero group-velocity solutions only if there are solutions with nearly zero phase velocity.